

# Nonlinear models based on leaf architecture traits explain the variability of mesophyll conductance across plant species

Milad Rahimi-Majd<sup>1</sup>, Alistair Leverett<sup>2</sup>, Johannes Kromdijk<sup>2</sup>, and Zoran Nikoloski<sup>1</sup>

<sup>1</sup>Universität Potsdam Institut für Biochemie und Biologie

<sup>2</sup>University of Cambridge Department of Plant Sciences

March 29, 2024

## Abstract

Mesophyll conductance ( $g_m$ ) describes the efficiency with which  $\text{CO}_2$  moves from substomatal cavities to chloroplasts. Despite the stipulated importance of leaf architecture in affecting  $g_m$ , there remains a considerable ambiguity about how and whether anatomy influences  $g_m$ . This is, in part, because studies exploring the relationship between leaf architecture and  $g_m$  have often relied on simple linear or exponential models to identify correlations. Here, we employed non-linear machine learning models to more comprehensively assess the relationship between ten leaf architecture traits and  $g_m$ . These models achieved excellent predictability of  $g_m$ , which depended on the leaf architecture traits considered as predictors. Dissection of the importance of leaf architecture traits in the models indicated that cell wall thickness and chloroplast area exposed to internal airspace have a large impact on interspecific variation in  $g_m$ . Additionally, other leaf architecture traits, such as: leaf thickness, leaf density, and chloroplast thickness emerged as important predictors of  $g_m$ . We found significant differences in the predictability between models trained on different plant functional types (PFTs): those trained on woody species could predict  $g_m$  by anatomical traits on other woody PFTs, ferns, and  $\text{C}_3$  herbaceous plants, whereas the converse did not hold in general. By moving beyond simple linear and exponential models, our analyses demonstrated that a larger suite of leaf architecture traits drive differences in  $g_m$  than has been previously acknowledged. These findings pave the way for modulating  $g_m$  by strategies that modify its leaf architecture determinants.

# **Nonlinear models based on leaf architecture traits explain the variability of mesophyll conductance across plant species**

Milad Rahimi-Majd<sup>1,2</sup>, Alistair Leverett<sup>3</sup>, Johannes Kromdijk<sup>3,4</sup>, and Zoran Nikoloski\*<sup>1,2</sup>

<sup>1</sup>Bioinformatics Department, Institute of Biochemistry and Biology, University of Potsdam, 14476 Potsdam, Germany

<sup>2</sup>Systems Biology and Mathematical Modeling Group, Max Planck Institute of Molecular Plant Physiology, 14476 Potsdam, Germany

<sup>3</sup>Department of Plant Sciences, University of Cambridge, Cambridge, Cambridgeshire, CB23EA, UK

<sup>4</sup>Carl R Woese Institute for Genomic Biology, University of Illinois at Urbana-Champaign, IL61801, Illinois, USA

\*Contact: [nikoloski@mpimp-golm.mpg.de](mailto:nikoloski@mpimp-golm.mpg.de)

Short title: Nonlinear models of mesophyll conductance

## Abstract

Mesophyll conductance ( $g_m$ ) describes the efficiency with which  $\text{CO}_2$  moves from substomatal cavities to chloroplasts. Despite the stipulated importance of leaf architecture in affecting  $g_m$ , there remains a considerable ambiguity about how and whether anatomy influences  $g_m$ . This is, in part, because studies exploring the relationship between leaf architecture and  $g_m$  have often relied on simple linear or exponential models to identify correlations. Here, we employed non-linear machine learning models to more comprehensively assess the relationship between ten leaf architecture traits and  $g_m$ . These models achieved excellent predictability of  $g_m$ , which depended on the leaf architecture traits considered as predictors. Dissection of the importance of leaf architecture traits in the models indicated that cell wall thickness and chloroplast area exposed to internal airspace have a large impact on interspecific variation in  $g_m$ . Additionally, other leaf architecture traits, such as: leaf thickness, leaf density, and chloroplast thickness emerged as important predictors of  $g_m$ . We found significant differences in the predictability between models trained on different plant functional types (PFTs): those trained on woody species could predict  $g_m$  by anatomical traits on other woody PFTs, ferns, and  $\text{C}_3$  herbaceous plants, whereas the converse did not hold in general. By moving beyond simple linear and exponential models, our analyses demonstrated that a larger suite of leaf architecture traits drive differences in  $g_m$  than has been previously acknowledged. These findings pave the way for modulating  $g_m$  by strategies that modify its leaf architecture determinants.

**keywords:** mesophyll conductance, leaf architecture traits, plant functional types, machine learning, non-linear regression models, impurity-based feature importance

## 1 Introduction

Mesophyll conductance,  $g_m$ , is a numerical measure of the rate of diffusion of  $\text{CO}_2$  from the substomatal cavities to RuBisCO, the site of carboxylation in the chloroplasts. An increase in mesophyll conductance is thus expected to elevate the rate at which RuBisCO can fix  $\text{CO}_2$ , thereby decreasing the water and nitrogen costs for carbon acquisition and fixation. Therefore, understanding factors controlling  $g_m$  is considered important for increasing the availability of  $\text{CO}_2$  at RuBisCO's site of carboxylation, with expected concomitant improvement in the rate of photosynthesis (Zhu et al., 2010).

Relatively few leaf anatomical traits have been linked to interspecific variation in  $g_m$ . Existing evidence has indicated that cell wall thickness,  $T_{cw}$ , and surface area of chloroplasts exposed to the intercellular airspaces per unit leaf area,  $S_c$ , are important determinants of  $g_m$ , as these traits negatively and positively correlate with  $g_m$ , respectively (Clemente-Moreno et al., 2019; Carriquí et al., 2020; Veromann-Jürgenson et al., 2020; Tosens et al., 2016; Veromann-Jürgenson et al., 2017 ; Gago et al., 2019 and references therein). However, there is still considerable ambiguity

36 regarding the extent to which  $T_{cw}$  and  $S_c$  affect  $g_m$ , as their predictive power can be weak or  
37 even nonsignificant. For example, (Xiong, 2023) found that neither of these anatomical traits  
38 correlated with  $g_m$  in  $C_3$  crops, using simple linear regression models. Furthermore, other studies  
39 presenting regression analyses on data collected from the literature (Flexas et al., 2021; Knauer  
40 et al., 2022a) have generally yielded weak models based on the two aforementioned anatomical  
41 traits for different plant functional types (PFTs). Whilst it is true that some exceptional cases have  
42 shown very high predictive power, these are based on only very few data points (e.g. seven), and  
43 thus the generalizability of these models remains unexplored (Peguero-Pina et al., 2017; Carriquí  
44 et al., 2020). In addition, it remains unclear if other leaf architecture traits, besides  $T_{cw}$  and  $S_c$ ,  
45 contribute to explaining variance of  $g_m$ .

46 The ambiguity surrounding the importance of anatomy is perhaps not surprising if one consid-  
47 ers that  $g_m$  is a composite parameter that integrates the effects of multiple factors, including: cell  
48 wall, plasma membrane (via its permeability, affected by aquaporins), cytosol, chloroplast enve-  
49 lope and stroma (Evans, 2021). This problem is further exacerbated by the differences in  $g_m$  values  
50 obtained by different measuring approaches. As leaf development will often be governed by allo-  
51 metric scaling rules (John et al., 2013), and anatomical traits may have antagonistic and/or complex  
52 impacts on  $g_m$ , it is likely that simple models based on one or two explanatory variables may be  
53 insufficient to robustly capture the relationships between anatomy and  $g_m$ . However, to date, the  
54 majority of models have applied this approach, describing the relationship between anatomy and  
55  $g_m$  have been based on single- and two-variable linear or exponential relationships.

56 Advances in machine learning approaches provide one suitable means to obtain data-driven  
57 insights in the determinants of  $g_m$ . Modern machine learning approaches can capture non-linear  
58 relationships, and comparisons of models built using different plant functional types (PFTs) can  
59 test the generalizability of the resulting models. Here, we used machine learning techniques to  
60 address four questions: (1) Can machine-learning approaches be used to improve the predictive  
61 power of models describing the relationship between anatomy and  $g_m$ ? (2) Do  $S_c$  and  $T_{cw}$  emerge  
62 as important determinants of  $g_m$  when several leaf architecture traits are used as inputs into non-  
63 linear models? (3) Can these non-linear models identify other leaf architecture traits (besides  $S_c$   
64 and  $T_{cw}$ ) influence  $g_m$ ? (4) Do the best fitting models vary between different PFTs, and are they  
65 generalizable?

66 To address these questions, we make use of the largest compendium of  $g_m$  values along with  
67 leaf cell architecture traits published to date, measured over different PFTs and species. These data  
68 allow us to also investigate and fully address the extent of generalizability of the developed non-  
69 linear models between different PFTs. Lastly, we show how exhaustive consideration of different  
70 combinations of predictors can help in characterizing the role of leaf cell architecture in the control  
71 of  $g_m$ , and, thereby, photosynthesis.

## 72 2 Results

### 73 2.1 Predictive performance of the random forest models within PFTs

74 To identify and analyze the relationships between leaf architecture traits and  $g_m$ , we used a recently  
75 published comprehensive data set (Knauer et al., 2022b) providing measurements of diverse leaf  
76 traits on the same set of plants. This is currently the largest available data set for  $g_m$ , collecting  
77 measurements from 563 peer-reviewed studies over 617 species partitioned into 13 major PFTs.  
78 To train random forest (RF) models, we then constructed all possible combinations of traits for the  
79 *global data set* (consisting of all PFTs) and for each of the individual PFTs, respectively. Further,  
80 we considered only those combinations with at least 50 samples, with no missing data, allowing  
81 us to avoid data imputation that may bias the findings (see section Data and preprocessing, for  
82 details).

83 Some of the random forest (RF) models (see section The model), assessed by cross-validation  
84 on the global data set, revealed excellent relationships between different combinations of leaf ar-  
85 chitecture traits and  $g_m$  across all PFTs and species (Fig. 1). The performance of the models,  
86 i.e. predictability, was assessed by the adjusted coefficient of determination,  $R_{adj}^2$ , that controls  
87 for the number of predictors, and the Pearson correlation coefficient,  $r$ , between the predicted and  
88 measured  $g_m$  values. We note that  $R_{adj}^2$  assesses the quantitative agreement, while  $r$  captures the  
89 qualitative agreement between the measured and predicted  $g_m$  values.

90 The model based on the combination of five anatomical traits, namely,  $T_{cw}$ ,  $S_c$ ,  $T_{leaf}$ ,  $T_{chl}$ ,  
91 and  $D_{leaf}$  (model 1 in Fig. 1), showed both quantitatively and qualitatively the best predictability  
92 ( $R_{adj}^2 = 0.63$  and  $r = 0.90$ ). Combinations involving some of these five traits were included as  
93 predictors in seven of the ten models ranked high with respect to their predictability (i.e., models  
94 2 – 5, 7, 8, and 10 in Fig. 1). Furthermore, the model that considered  $T_{cw}$  and  $S_c$  (model 14 in Fig.  
95 1), the model that considered  $T_{cw}$ ,  $T_{leaf}$ , and  $D_{leaf}$  (model 3 in Fig. 1), and the one based on the  
96 combination of  $T_{cw}$ ,  $S_c$ ,  $T_{chl}$ , and  $D_{leaf}$  (model 4 in Fig. 1) were the best-performing among those  
97 trained on two to four anatomical traits as predictors.

98 The best-performing model ( $R_{adj}^2 = 0.55$  and  $r = 0.89$ ) based on a combination of six traits  
99 included:  $T_{cw}$ ,  $S_c$ ,  $T_{leaf}$ ,  $T_{chl}$ ,  $D_{leaf}$ , and  $S_m$ , while the best-performing model ( $R_{adj}^2 = 0.49$  and  
100  $r = 0.88$ ) on seven traits included:  $LMA$ ,  $T_{mes}$ ,  $T_{cw}$ ,  $T_{chl}$ ,  $S_m$ ,  $S_c$ , and  $T_{leaf}$ . Interestingly, the  
101 best-performing model ( $R_{adj}^2 = 0.22$  and  $r = 0.85$ ) with eight traits, namely:  $LMA$ ,  $T_{mes}$ ,  $T_{cw}$ ,  
102  $T_{cyt}$ ,  $T_{chl}$ ,  $S_m$ ,  $S_c$ , and  $T_{leaf}$  ( $R_{adj}^2 = 0.22$  and  $r = 0.85$ ), was considerably weaker in comparison  
103 to the top performing models with fewer traits as predictors.

104 This raised the question of why the introduction of additional predictors did not result in a  
105 further increase in model performance. The considerably smaller number of models on six or more  
106 traits in comparison to the number of models based on five traits (i.e. 80 models with six traits, 19

107 models with seven, one model with eight, and no models with nine or ten traits in comparison to  
108 157 models on five traits) seemed as a plausible explanation (see section Data and preprocessing).  
109 To address the concern about the data limitations for models that include more than five traits as  
110 predictors, we then considered a different data-splitting approach. To this end, we used a smaller  
111 value (of 25 rather than 50) for the minimum number of data points required for a combination of  
112 traits, and performed the same model training and cross-validation. In this robustness analysis, we  
113 did not use  $R_{adj}^2$  as a performance measure since the number of traits and test data points was equal  
114 or close to each other for some trait combinations, resulting in infinity or out-of-bound values for  
115  $R_{adj}^2$ . Interestingly, the traits contributing to the best model with respect to the  $r$  values were the  
116 same as in the previous analysis; in addition, other models with at most six traits again displayed  
117 high performance scores (Fig. S1). Therefore, the robustness analysis indicated that the models on  
118 a larger number of traits as predictors did not outperform the best model with five traits, identified  
119 based on the stricter data consideration.

120 Other factors that can contribute to a poor performance of a RF model include (multi)collinearity  
121 of predictors and presence of irrelevant predictors. In other words, adding irrelevant and highly  
122 correlated predictors is not expected to improve model performance and may also have an opposite  
123 effect on model performance due to the increasing model uncertainty and complexity (Kuhn et al.,  
124 2013). Indeed, we found pairwise correlations between different traits, indicating their collinearity  
125 (Fig. 2a). For example,  $T_{leaf}$  and  $T_{mes}$ ,  $T_{leaf}$  and  $LMA$ ,  $D_{leaf}$  and  $LMA$  as well as  $T_{mes}$  and  $LMA$   
126 represent trait pairs showing strong, moderate, weak, and no correlations, respectively (Fig. S2).  
127 Thus, (multi)collinearity of the predictors can explain the negative effect of increasing number of  
128 predictors on the performance of RF models.

129 Feature selection is a common strategy to resolve the problem of (multi)collinearity among the  
130 predictors. This is performed either by preselecting the predictors according to defined criteria (fil-  
131 ter methods) or by iteratively identifying the predictors that maximize the performance of the target  
132 model (wrapper methods) (Kuhn et al., 2013). Both approaches aim to remove non-informative  
133 and highly correlated traits and reach an optimal subset with respect to different criteria (e.g. min-  
134 imum number of predictors retained). In our setting, having only ten predictors allowed us to  
135 investigate all possible combinations of predictors along with the respective models. As a result,  
136 we did not rely on selection of features since we performed exhaustive training of models of each  
137 of these combinations of predictors. We expected the five traits appearing in our best-performing  
138 model (model 1 in Fig. 1) to be the best representatives for the rest of the traits and have no  
139 high correlations with each other. Indeed, as expected, we found that all pairs of predictors in the  
140 best-performing model show weak correlations, except for  $D_{leaf}$  and  $T_{cw}$  that exhibit moderate  
141 correlations (Fig. 2b). In addition, removing  $D_{leaf}$  from the set of predictors resulted in the second  
142 best-performing model ( $R_{adj}^2 = 0.61$ , model 2 in Fig. 1). This demonstrates that  $D_{leaf}$ , despite the

143 moderate correlations to the other predictors, still contributes to explaining some of the variance in  
144  $g_m$ . Therefore, our modeling strategy contributed to understanding how (multi)colinearity between  
145 leaf architecture traits impacts on the predictability of the resulting models.

146 To better assess the last claim, we observed that a trait can be excluded from a model either  
147 because it is correlated to another predictor present in the model or because it does not contribute to  
148 explaining variance in  $g_m$ . Inspection of models for all possible combinations of traits as predictors  
149 allows us to assess the reasons for not considering a trait in a predictive model for  $g_m$ . Having more  
150 models with a positive  $R_{adj}^2$ , with different combination of traits, indicate one or both of the two  
151 possibilities: *i*) more traits significantly contribute to explaining variance in  $g_m$ , and *ii*) correlated  
152 traits also contribute to explanation of variance in  $g_m$ , due to lack of high correlation between  
153 each other. In this way, the number of models with positive  $R_{adj}^2$  and the distribution of their  
154 predictability values provide a general view in assessing the relationship between leaf anatomy and  
155  $g_m$ . The information provided by this metric can also be more robust than the information obtained  
156 by the best-performing model, considering the possible overfitting due to the number of data points  
157 and biological differences between species appearing in each model (i.e. trait combination).

158 Following this logic, we summarized the information about the performance of the models on  
159 the global data set and on data of individual PFTs using the distribution of predictability scores  
160 (Fig. 3). In addition to the global data set (as discussed above), the cross-validation over the data  
161 of eight individual PFTs showed several models with non-negative  $R_{adj}^2$ . For instance, woody ev-  
162 ergreens, woody evergreen angiosperms, gymnosperms, evergreen gymnosperms,  $C_3 - C_4$  herba-  
163 ceous, woody angiosperms,  $C_3$  herbaceous, and extended ferns were the PFTs with at least one  
164 model with positive  $R_{adj}^2$ . Excluding  $C_3$  herbaceous, the best models of the mentioned PFTs  
165 showed weak to moderate  $R_{adj}^2$  scores alongside high values for  $r$  between the measured and pre-  
166 dicted values of  $g_m$  in the test set (Table 1). These results provide further, strong evidence for the  
167 effect of leaf anatomy on  $g_m$  within PFTs, in agreement with what has already been presented in  
168 the literature (e.g., Knauer et al., 2022a).

169 However, these results raise the question of why there are such differences in the predictive  
170 performance scores between the global data set and the PFTs, as well as between the PFTs them-  
171 selves. To address this issue, we aimed to further examine the clear statistical differences in the  
172 data of the different PFTs. We observed that data from individual PFTs contained fewer data points  
173 compared to the global data set, which, as mentioned above, can negatively affect the performance  
174 of the models when trained on the data from the individual PFTs. Moreover, the data sets of each  
175 of the considered PFTs omit some traits, resulting in the consideration of only a fraction of the  
176 possible combinations with the ten traits as predictors (Table S2).

177 To investigate the effect of missing traits and combinations, we focused on the most special  
178 case, that of  $C_3$  herbaceous PFT, which showed very poorly performing models ( $R_{adj}^2 \leq 0.04$ )

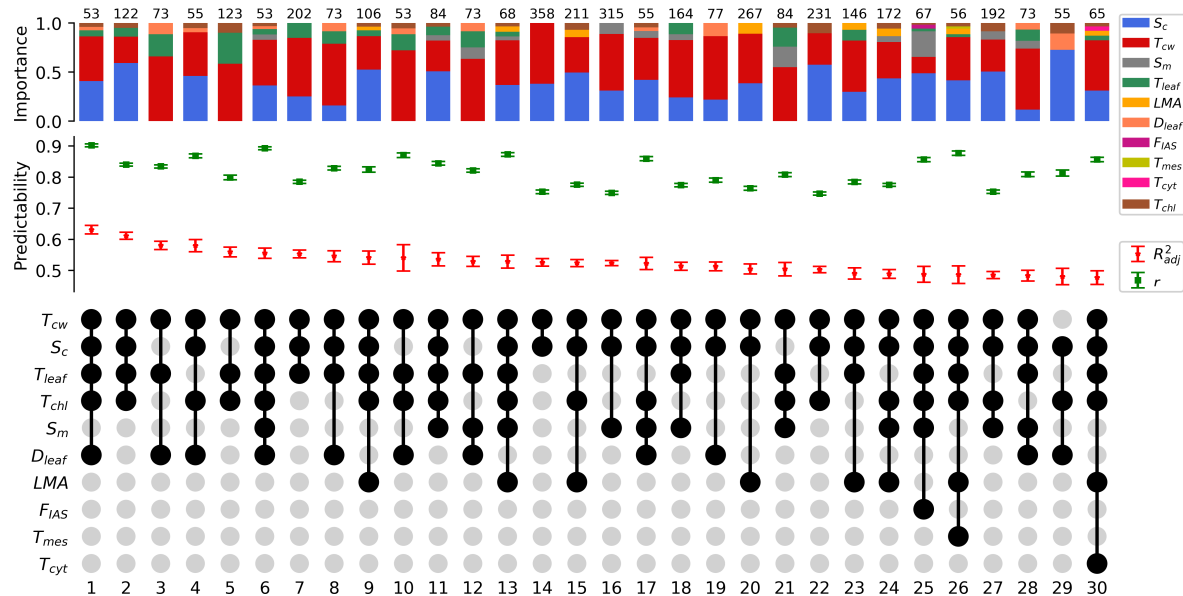


**Figure 1: Predictive performance of random forest models using different combinations of leaf anatomical traits.** The UpSet plot shows the predictability evaluation of top 30 models for  $g_m$ , based on average  $R_{adj}^2$ , consisting of ten anatomical traits  $LMA$ ,  $T_{mes}$ ,  $F_{IAS}$ ,  $T_{cw}$ ,  $T_{cyt}$ ,  $T_{chl}$ ,  $S_m$ ,  $S_c$ ,  $T_{leaf}$ , and  $D_{leaf}$  over all available species and PFTs of Knauer et al. (2022b) data set. The lower panel shows the intersection of traits contributing to the training model. The middle panel indicates the average  $R_{adj}^2$  and  $r$  between the measured and predicted values of  $g_m$  in the test set. The error bars show the standard errors of the predictability measures. The upper panel shows the average Gini importance of the corresponding traits at each combination of the traits. The number of data points in each model is provided above the importance bars. For all models, the average predictability scores were achieved by the RF model in 150 executions, with 70% randomly chosen data elements used for the training set and the remaining 30% used for the test set.

179 across the 49 trained models. To this end, we applied the same analyses to the data set of a recently  
 180 published paper (Xiong, 2023), providing the  $g_m$  data for eight of our anatomical traits across ten  
 181  $C_3$  crops. This yielded several models with considerably higher predictive performance for  $C_3$   
 182 herbaceous plants, i.e., moderate  $R_{adj}^2$  and high  $r$  values, where at least one of the traits involved in  
 183 each of the top 30 models was missing in our  $C_3$  herbaceous data set (Fig. S3). The observed effect  
 184 of missing traits and combinations in this particular case, along with strong correlation values  
 185 in all PFTs, suggests that increasing the available data for individual PFTs may improve model  
 186 performance.

## 187 2.2 Predictive performance of the RF models between PFTs

188 Our other approach to assess the relationships between leaf structural traits and  $g_m$  was cross-  
 189 prediction over PFTs, i.e., prediction of the  $g_m$  values in one PFT by the RF models trained on the  
 190 data set of another PFT. This approach allowed us to assess if and to what extent the models are

**Table 1: Best-performing models for  $g_m$  in cross-validation within different PFTs.**

PFT	$R_{adj}^2$	$r$	$n$
Global data set	0.63	0.90	599
Woody evergreens	0.42	0.75	72
Woody evergreen ang.	0.3	0.74	63
$C_3 - C_4$ herbaceous	0.37	0.69	49
Evergreen gym.	0.3	0.41	31
Extended ferns	0.22	0.78	7
Woody angiosperms	0.21	0.68	72
$C_3$ herbaceous	0.04	0.51	49

Cross-validation predictability scores of the model with the highest  $R_{adj}^2$  for global data set and each of seven individual PFTs with at least one model with positive  $R_{adj}^2$ . The number of trained models,  $n$ , for each data set is also given in the table.

191 generalizable, i.e. their performance remains good on unseen data sets. This modeling strategy also  
 192 sharply decreases the probability that a pair of data samples from an identical study is split such that  
 193 one lies in the training set and the other on the test set, given the majority of the studies in the data  
 194 set provide measured  $g_m$  for a few species from one PFT. As a result, this strategy overcomes the  
 195 bias in the models due to possible systematic errors in measurements of different studies. Finally,  
 196 by following this strategy, we aimed to investigate if the same relationship, captured in a RF model,  
 197 holds across PFTs.

198 First, we developed RF models in a setting where the data of one PFT was considered as  
 199 the test set and the remaining data as the training set. This resulted in numerous models with  
 200 moderate to strong  $R_{adj}^2$  and  $r$  values (Fig. 4a). The prediction of  $g_m$  on woody angiosperms,  
 201 including both evergreen and deciduous species, showed the largest number of RF models with  
 202 a positive  $R_{adj}^2$  set as well as the model with the highest predictability across all scenarios (Fig.  
 203 4a and Table 2). The two subgroups of these species, woody evergreen angiosperms and woody  
 204 deciduous angiosperms, also showed several models with moderate  $R_{adj}^2$  and strong  $r$  values. A  
 205 special case was the scenario with  $C_3$  annual herbaceous as the test set, which showed a weak  
 206 performance for one model and a negative  $R_{adj}^2$  for the rest of 347 trained models. This finding  
 207 distinctly contrasts the scenario in which  $C_3$  perennial herbaceous was considered as a test set,  
 208 showing several models with moderate to strong predictability scores on only 83 trained models.  
 209 In addition, the union of these PFTs, i.e.,  $C_3$  herbaceous and  $C_3 - C_4$  herbaceous, as the test  
 210 sets also showed predictability scores with performances between these two cases. The prediction  
 211 of  $g_m$  on evergreen gymnosperms and woody evergreens as test sets showed 28 and four models  
 212 with a positive  $R_{adj}^2$ , respectively. Finally, the scenarios with the (extended) ferns as the test sets  
 213 also showed ten models with non-negative  $R_{adj}^2$ , with the best models showing moderate to strong

214 predictability scores. The data on the remaining PFTs either did not result in a model with non-  
215 negative  $R_{adj}^2$  or did not contain sufficient points to apply the same prediction scenarios (Table  
216 S2).

217 In the next step, we investigated prediction scenarios in which the different pairs of non-  
218 overlapping PFTs were considered as the training and test sets for the RF models, respectively.  
219 Among all the possible pairs of PFTs, 121 scenarios had at least one combination of traits with  
220 sufficient training and test data points, with 31 of them resulting in at least one model with pos-  
221 itive  $R_{adj}^2$  values (Fig. 4b and Fig. S4). Different groups of woody plants, i.e., woody (ev-  
222 ergreen/deciduous) angiosperms and evergreen gymnosperms,  $C_3$  (annual/perennial) herbaceous  
223 plants, and (extended) fern plants were included in the training and the test sets of all 31 scenarios.

224 The RF models trained on data from selected woody species and tested on the other woody  
225 species,  $C_3$  herbaceous plants, and ferns were generally the best-performing (Fig. 4b, Fig. S4 and  
226 Table 2).

227 Woody angiosperm species represented a special case, since: (i) the model trained on the global  
228 set (excluding this PFT) resulted in the best-performing model when tested on this PFT (Table 2)  
229 and (ii) the model trained on data from this PFT predicted  $g_m$  with the best performance on data  
230 from  $C_3$  perennial herbaceous species (Table 2). In addition, models trained on data from woody  
231 plants resulted in 40 models with positive  $R_{adj}^2$  when tested on data from (extended) ferns (Fig.  
232 4b and S4). However, the models trained on (extended) ferns could only predict  $g_m$  on  $C_3$  ( $-C_4$ )  
233 herbaceous and woody plants in 8 and 2 models, respectively. On the other hand, the models trained  
234 on  $C_3$  herbaceous plants could only predict the  $g_m$  from the other  $C_3$  herbaceous plants (15 models)  
235 and woody deciduous plants (2 models). The scenarios with the  $C_3$  perennial herbaceous as the  
236 test sets showed several models with positive  $R_{adj}^2$ , including the one with the best predictability  
237 scores. However, this was not the case for the  $C_3$  annual herbaceous. This result was in line with  
238 the significant difference between the predictability of the models tested on  $C_3$  annual herbaceous  
239 and  $C_3$  perennial herbaceous, both of which were trained on the rest of the global data set (Table  
240 2).

### 241 **2.3 Importance of anatomical traits in predicting $g_m$**

242 The relative importance of the traits contributing to the RF models is of particular interest when  
243 interpreting the nonlinear relationships between anatomical traits and  $g_m$ .

244 Previous works investigating the relationships between  $g_m$  and leaf architecture generally con-  
245 sidered and investigated models with one or two traits. They then identified the traits with and  
246 without significant regression scores as important and unimportant, respectively (e.g., Knauer  
247 et al., 2022a, Flexas et al., 2021, Xiong, 2023). However, here we follow a different approach:  
248 we developed a model for each possible combination of ten traits, available in our data set, and

249 computed the performance of the RF models in predicting  $g_m$  by anatomical traits. Hence, we  
250 required different strategies to identify which traits were more important in explaining  $g_m$ . To this  
251 end, we considered three different aspects to evaluate the importance of the traits: *i*) the contri-  
252 bution of a trait in the given model, *ii*) the relative importance of a contributing trait in the given  
253 RF model, and *iii*) the overall impact of a trait in a set of models in terms of its contribution and  
254 relative importance, taking into account the performance of the models containing the trait.

255 The traits contributing to the optimal model can initially be considered as the most important in  
256 explaining  $g_m$ . However, the contribution of a trait still does not provide details about its share in  
257 predicting the  $g_m$  in the optimal model. Therefore, we considered the average impurity-based Gini  
258 importance of each trait across different runs of the RF model as its relative importance (Fig. 5).  
259 The first surprising result was the major share of importance of one or two traits included in each  
260 model. Further, in most models, one trait accounted for at least 50% of the Gini importance and  
261 another trait accounted for most of the remaining portion. Interestingly,  $S_c$  and  $T_{cw}$  were among  
262 the important traits in the majority of models. This is in line with several previous works that  
263 recognized these traits as the two essential anatomical traits to explain the variation of  $g_m$  across  
264 PFTs and species (see Section Introduction). In addition, each of the other eight traits contributed  
265 to at least one of the best-performing models. This provides evidence that the ten investigated  
266 anatomical traits contribute to explaining the variance in  $g_m$  across plant species.

267 Next, we investigated the contribution and importance of the traits in other RF models. Similar  
268 to the best-performing, the remaining models with a non-negative performance showed a large  
269 proportion of Gini importance for only one or two traits (e.g., the upper panel of Fig. 1, S1).  
270 To summarize the importance of each trait over all the models with positive  $R_{adj}^2$  we used two  
271 total importance measures  $IMP_C$  and  $IMP_G$  (see Section Measures of predictor importance in RF  
272 models). Interestingly, except in three cases (i.e., the scenario trained on the  $C_3$  annual herbaceous  
273 and tested on  $C_3$  perennial herbaceous plants along with the scenarios trained on  $C_3$  and  $C_3 - C_4$   
274 herbaceous and tested on woody deciduous angiosperms), one or both of  $S_c$  and  $T_{cw}$  were again  
275 the most important traits based on  $IMP_G$  in all the scenarios (Fig. 3, 4a, 4b, and S4). However,  
276 the ordering of traits based on importance values assessed by  $IMP_C$  were different: in ten cases,  
277 neither  $S_c$  nor  $T_{cw}$  were found to be among the top two important traits, and the importance share  
278 of the most important traits small compared to the results obtained by  $IMP_G$ . Excluding  $S_c$  and  
279  $T_{cw}$ , again, all the remaining eight traits showed a considerable contribution of total importance, at  
280 least in one of the prediction scenarios, particularly when using  $IMP_C$ . As special cases,  $D_{leaf}$  and  
281  $S_m$  were the most important traits in two scenarios, and  $LMA$  and  $f_{IAS}$  were the most important in  
282 one scenario in terms of both measures of total importance.

283 In summary, our findings indicated that the ten considered anatomical traits are important in  
284 explaining  $g_m$  in different prediction scenarios, based on considering the best-performing models

285 or all the models with a positive  $R_{adj}^2$ . We also showed that the relative importance of a few  
286 of the traits in explaining  $g_m$  is considerably higher than the others. Meanwhile, there are still  
287 uncertainties in ranking the importance of the traits due to data limitations. More specifically,  
288 except for two prediction scenarios (i.e., cross-validation over the global data set and the scenario  
289 with woody angiosperms as the test set and the rest of the global data set as the training set), one  
290 or more traits were missing in other scenarios. Therefore, we avoid ranking the contribution of the  
291 traits and only highlight the main trends, such as the major importance of the two traits, namely,  
292  $S_c$  and  $T_{cw}$ .

### 293 **3 Discussion**

294 Our study aimed to address the relationship between leaf architecture traits and  $g_m$ , thus helping  
295 assess the suitability of modulating leaf anatomy as a way towards engineer  $g_m$ . Several studies  
296 have already investigated and attempted to find significant empirical relationships between leaf  
297 architecture traits and variability of  $g_m$  across plant species. The models reported in the existing  
298 studies mainly suggested that two anatomical traits,  $T_{cw}$  and  $S_c$ , can explain a small proportion  
299 of the variability in  $g_m$ , as assessed by weak to moderate  $R^2$ ; these models were developed often  
300 using a limited number of data points (see section Introduction). In addition, these modelling  
301 efforts generally failed to find a significant relationship between leaf structural traits (e.g.,  $LMA$ ,  
302  $D_{leaf}$ ,  $T_{leaf}$ , and  $T_{mas}$ ) and variation of  $g_m$  across PFTs and species (Knauer et al., 2022a). As a  
303 result, the existing models tend to not generalize well on unseen data. Further, the existing models  
304 are rooted in different linear and nonlinear regression approaches. For instance, different studies  
305 have used linear (Carriquí et al., 2020), exponential (Tosens et al., 2016), logarithmic (Tomás et al.,  
306 2013; Veromann-Jürgenson et al., 2017, 2020), and power-law (Flexas et al., 2021; Knauer et al.,  
307 2022a) models to fit the  $g_m$  based on  $T_{cw}$ .

308 However, comprehensive models that consider the majority of measured leaf architecture traits  
309 as predictors have not yet been carefully investigated and compared. Here, we ask if non-linear  
310 machine-learning models, with more than two leaf architecture traits as predictors, can be used  
311 to improve the predictive power of models describing the relationship between anatomy and  $g_m$ .  
312 Interestingly, the RF model built based on data for the two anatomical traits,  $T_{cw}$  and  $S_c$ , found  
313 moderately correlated with  $g_m$ , demonstrated that increases in any of these traits does not neces-  
314 sarily lead to an increase in  $g_m$  (see the rugged surface on Fig. S5). This was a further motivation to  
315 employ multivariate nonlinear models that consider other anatomical and structural traits describ-  
316 ing different parts of leaf architecture. In this regard, we created an RF model for each possible  
317 combination of ten leaf architecture traits on the available data across 34 distinct prediction sce-  
318 narios, representing the global data set, different PFTs, and combinations thereof.

319 Following these strategies, we identified several models, considering both anatomical and  
320 structural traits, with strong predictability scores for different prediction scenarios. Particularly,  
321 we found that the model trained on all the PFTs can predict  $g_m$  based on three anatomical traits  
322 (i.e.,  $T_{CW}$ ,  $S_C$ , and  $T_{chl}$ ) and two structural traits (i.e.,  $D_{leaf}$ , and  $T_{leaf}$ ) over unseen data with  
323  $R_{adj}^2 = 0.63$  and  $r = 0.9$ . This evidence reliably indicates that the leaf architecture is a primary de-  
324 terminant of the variation of  $g_m$  within and between PFTs. Furthermore, these findings suggest that  
325 a comprehensive analysis of both leaf structure and anatomy is necessary to explain the variation of  
326  $g_m$  across species. On the other hand, our analysis indicated that in addition to the best-performing  
327 model for each scenario, other models based on different combinations of the traits should also  
328 be taken into account. This can result in an exhaustive understanding of different aspects of the  
329 effect of leaf architecture on  $g_m$ , considering weak to strong (but not perfect) correlations between  
330 anatomical and structural traits.

331 The aim of this study was to also provide robust and generalizable models allowing to assess the  
332 extent to which different parts of the leaf architecture associate to  $g_m$  across PFTs and species. To  
333 this end, we also examined whether and how the models trained on one or more PFTs can predict  
334  $g_m$  from other, unseen PFTs. This resulted in the identification of the most robust models tested  
335 on completely unseen species. Moreover, this strategy can uncover similarities and differences  
336 in the association of  $g_m$  with leaf architecture across different PFTs. Our results yielded strong  
337 predictability for several models built based on this idea. For instance, the models trained on  
338 the global data set, with no overlap with the test sets, could predict  $g_m$  on woody angiosperms,  
339  $C_3$  herbaceous, and (extended) ferns with an  $R_{adj}^2 > 0.5$ . On the other hand, among the models  
340 trained and tested on individual PFTs, the ones either trained or tested on woody plants generally  
341 showed higher performances. The models trained on data from these plants could predict  $g_m$  on  
342 other woody plants,  $C_3$  herbaceous plants, and ferns. However, the models trained on data from  
343 ferns and  $C_3$  annual herbaceous generalized to a much smaller degree to other PFTs.

344 Interestingly, our analysis of the data from Xiong (2023) found that only two of the 30 best-  
345 performing models contained both  $T_{cw}$  and  $S_c$  as, with these traits making up only a small fraction  
346 of the Gini importance scores (Fig. S3). This outcome varies considerably from the analysis based  
347 on the Knauer et al. (2022b) data set including all PFTs (Fig. 1). Furthermore, the observation that  
348  $T_{cw}$  seems less important in the crop species studied by Xiong (2023) is in stark contrast with a  
349 published comparison of anatomy across 15 species, spanning multiple PFTs. Tomás et al. (2013)  
350 showed that the slope between  $g_m$  (standardised by  $S_c$ ) and  $T_{cw}$  was much steeper within herba-  
351 ceous  $C_3$  species, than for evergreen trees, suggesting that  $T_{cw}$  plays a larger role in determining  
352  $g_m$  within the  $C_3$  herbaceous annual leaves. The importance of  $T_{cw}$  in determining  $g_m$  has also  
353 been difficult to assess from experimental studies. For example, work on tobacco found that the  
354 reduction in  $g_m$  coinciding with leaf age was strongly correlated with an increase in  $T_{cw}$  (Clarke

355 et al., 2021). However, knocking down cell wall mixed-linkage glucan production in rice plants  
356 resulted in lower  $g_m$ , alongside concurrent reductions to  $T_{cw}$  (Ellsworth et al., 2018). As a result  
357 of these contrasting observations, it remains unclear if, and to what extent,  $T_{cw}$  is influencing  $g_m$   
358 within  $C_3$  herbaceous annuals.

359 One open question from this study is why models to describe  $C_3$  annual plants underperformed,  
360 compared to other PFTs. One possible explanation is that this is an artifact, caused by the aver-  
361 aging of  $g_m$  values derived from different experimental methods. Knauer et al. (2022a) showed  
362 that linear regressions between  $g_m$  and  $V_{cmax}$  fit the data considerably better when separate mod-  
363 els were built depending on the method used to estimate  $g_m$  (i.e. isotope, fluorescence or curve  
364 fitting). Whilst  $V_{cmax}$  bears no importance for our analysis, this indicates that averaging  $g_m$  val-  
365 ues may not always yield the most reliable results. Estimations of  $g_m$  rely on several assumptions  
366 (e.g., fractionation factors, the photorespiratory compensation point, methods chosen to estimate  
367 respiration). As such, it is conceivable that combining independent estimations of  $g_m$  may have  
368 introduced unforeseen errors into the dataset that may interfere with model construction. Given  
369 that there is a bias towards research on  $C_3$  annual species (which the majority of the world’s staple  
370 crop species belong), a greater number of measurements have been recorded, per species, for this  
371 PFT. Consequently, within the data set collated by Knauer et al. (2022b)  $C_3$  annual herbaceous  
372 species had 538 measurements for 52 species, whereas the ratio of measurements to species was  
373  $< 2.5$  for all other PFTs. This remains to be tested, but it may also explain why models could be  
374 built to describe the relationship between anatomy and  $g_m$  based on data from Xiong (2023), as  
375 these were derived from a single source and were not subject to the same averaging.

## 376 4 Conclusions

377 By using well-established machine learning approach, that of random forest, we demonstrated  
378 that one can obtain models based on leaf architecture traits that achieve excellent predictability of  
379  $g_m$ . In addition, we showed that these models are generalizable, particularly if trained with data  
380 from specific PFTs. We also presented a systematic approach for determining the importance of  
381 anatomical and structural traits based on the Gini importance of traits in best-performing models  
382 and two total importance measures that consider all models with a positive  $R_{adj}^2$  in each predic-  
383 tion scenario. Using the systematic approach, we found that not only  $T_{cw}$  and  $S_c$  are two critical  
384 traits in explaining the variation of  $g_m$  across plant species, but the remaining eight structural and  
385 anatomical traits considered play a role in explaining  $g_m$ . In future work, our approach can also  
386 be used for the exact ranking of the importance of the traits by increasing the data availability or  
387 considering natural variability within species.

## 5 Methods

### 5.1 Data and preprocessing

To identify and analyze the relationships between anatomical traits and  $g_m$ , we used a recently published comprehensive data set (Knauer et al., 2022b) providing leaf structural, anatomical, biochemical, and physiological traits measured on the same set of plants. This is currently the largest available data for  $g_m$ , which collected measurements from 563 peer-reviewed studies over 617 species partitioned to 13 major PFTs, namely: evergreen gymnosperms, deciduous gymnosperms, woody evergreen angiosperms, woody deciduous angiosperms, semi-deciduous angiosperms, CAM plants, ferns, fern allies, mosses,  $C_3$  perennial herbaceous,  $C_3$  annual herbaceous,  $C_4$  annual herbaceous, and  $C_4$  perennial herbaceous.

Since most of the individual PFTs do not contain enough data points to train a model for many of the possible combinations of the traits as predictors, we also formed five more groups from the union of the above PFTs. This was performed according to the shared functional characteristics among the PFTs. The groups involved the following: woody evergreens (union of woody evergreen angiosperms and evergreen gymnosperms), woody angiosperms (union of woody evergreen angiosperms, woody deciduous angiosperms, and semi-deciduous angiosperms), extended ferns (union of ferns and fern allies),  $C_3$  herbaceous (union of  $C_3$  perennial herbaceous and  $C_3$  annual herbaceous), and ( $C_3 - C_4$ ) herbaceous (union of  $C_4$  annual herbaceous,  $C_4$  perennial herbaceous,  $C_3$  perennial herbaceous, and  $C_3$  annual herbaceous). This strategy allowed us to not only increase the data available for model training, but also to compare the findings for different groups and their subgroups. This modeling strategy also facilitated the investigation of whether or not the combination of data from PFTs increase the generalizability of the models.

In our analyses, we used  $g_m$  values standardized to temperature of  $25^\circ C$  and atmospheric pressure of 1 bar ( $10^5 Pa$ ), as provided in the data set (see Knauer et al., 2022a). The data set contains information about all the published methods for estimating  $g_m$  in each study. Except for a few cases, all collected measurements were based on one of three methods: isotope (Evans et al., 1986; Caemmerer and Evans, 1991; Lloyd et al., 1992; Scartazza et al., 1998; Tazoe et al., 2009, 2011; Evans and Von Caemmerer, 2013; Mizokami et al., 2015), fluorescence (Harley et al., 1992; Loreto et al., 1992; Epron et al., 1995; Maxwell et al., 1997; Bernacchi et al., 2002; Yin and Struik, 2009; Yin et al., 2009), and curve fitting (Ethier and Livingston, 2004; Ethier et al., 2006; Sharkey et al., 2007; Gu et al., 2010; Sharkey, 2015). To have only one value for each individual experiment, we aggregated the repeated data by calculating per-species  $g_m$  as the average of its values measured with the different methods. After aggregation, we used all the remaining data with no additional filters.

The data sets includes measurements for 31 anatomical traits. However, in addition to the two

423 frequently reported traits ( $T_{cw}$  and  $S_c$ ), we selected eight other anatomical and structural traits  
424 that have received the most attention in the literature in terms of published data (Table S1): Leaf  
425 dry mass per area ( $LMA$ ), leaf density ( $D_{leaf}$ ), leaf thickness ( $T_{leaf}$ ), mesophyll thickness ( $T_{mes}$ ),  
426 cytosol thickness ( $T_{cyt}$ ), chloroplast thickness ( $T_{chl}$ ), surface area of mesophyll cells exposed to  
427 the intercellular airspaces per unit leaf area ( $S_m$ ), and fraction of intercellular airspaces in leaf  
428 mesophyll ( $F_{IAS}$ ). In this way, we kept all the data samples with a value for standardized  $g_m$  and  
429 *at least one* of the mentioned anatomical traits, resulting in 882 data samples from 453 species and  
430 all the mentioned PFTs. The number of data samples and species for individual PFTs and groups  
431 are provided in Table S2.

432 To investigate the performance of selected models, we used the data set from Xiong (2023)  
433 consisting of eight anatomical and structural traits  $T_{mes}$ ,  $F_{IAS}$ ,  $T_{cw}$ ,  $T_{cyt}$ ,  $T_{chl}$ ,  $S_m$ ,  $S_c$ , and  $T_{leaf}$   
434 measured for ten  $C_3$  crops. The measurements of  $g_m$  in this data set were obtained using online  
435 carbon isotope discrimination and chlorophyll fluorescence methods, and we used the  $g_m$  provided  
436 by the second method in our analyses.

437 To perform the model training based on data for each PFT, we then constructed all possible  
438 combinations of traits for the *global data set* (consisting of all PFTs) and for each of the individual  
439 PFTs, respectively. In each combination, we removed the data samples with a missing value in one  
440 or more traits. We then kept only the combinations with at least 50 data samples, with no missing  
441 data, and ignored the rest. This strategy allowed us to avoid data imputation, that may bias the  
442 findings given that the measurements are made across different plant species. Future studies may  
443 consider investigating the effect of bias by relying on recently proposed imputation techniques  
444 (Ellington et al., 2015; Scherer and Emslander, 2023; Lee and Beretvas, 2023). This resulted in  
445 599 combinations for the set of all PFTs, each containing from one to ten anatomical traits as  
446 independent variables and the corresponding standardized  $g_m$  as a response variable (Table S2).  
447 We also ensured that the training set was larger than the test set, to achieve generalizable models.

## 448 **5.2 The model**

449 The random forest (RF) model in a regression setting (Breiman, 2001) was used to predict  $g_m$   
450 by the anatomical traits, used as predictors. To achieve a robust result for the prediction scenar-  
451 ios within PFTs, for each combination of predictors we performed the training in a Monte-Carlo  
452 cross-validation setting (Smyth, 1996), by running 150 independent executions with 70% randomly  
453 chosen data points for the training set and the remaining 30% used for the test set. We also run  
454 the RF model 150 times for prediction scenarios between PFTs, with fixed training and test sets, to  
455 capture the effect of different random seeds controlling the bootstrapping and feature sampling in  
456 the trees (Raste et al., 2022). The training models and splitting data were implemented using the  
457 Python package Scikit-learn (Pedregosa et al., 2011). The source code ensuring reproducibility of

our analyses is available on GitHub: [github.com/MRahimiMajd/leaf\\_gm\\_architecture](https://github.com/MRahimiMajd/leaf_gm_architecture).

The predictive performance of the models was assessed quantitatively and qualitatively by using the coefficient of determination ( $R_{adj}^2$ ) and Pearson correlation ( $r$ ), respectively. The coefficient of determination ( $R^2$ ) is used as a quantitative measure of how much variance in  $g_m$  is explained by the anatomical traits, employed as predictors. However, our models have different numbers of independent variables (i.e., anatomical traits as predictors). To capture the effect of this difference on the performance of models, we relied on the  $R_{adj}^2$ , which adjusts the  $R^2$  value based on the number of predictors (Hocking, 1976).

### 5.3 Measures of predictor importance in RF models

To assess the relative importance of a trait contributing to a RF model, we used the impurity-based feature importance (Gini importance). Since the RF model is an ensemble of decision trees (obtained by node splitting), Gini importance measures the total reduction of the impurity of the RF model attributed to that feature, averaged over all trees in the ensemble (Pedregosa et al., 2011). For a single run or an ensemble of runs, we ensure that the (average) values of the relative importance of the contributing traits always sum up to one, as explained in the following.

For the case where we have several models with different combinations of traits as predictors, we are interested in obtaining a total importance for each trait across all these models. In our analyses, the number of models is given by the number of possible combinations of traits. However, poorly performing models do not provide any information about trait importance. Thus, by excluding these models, based on a threshold for the measure of performance, the number of models that include a given trait can simply be used as a measure of total importance for the trait. While seemingly sound, this measure does not discriminate between models of weak, moderate, and strong performance. To address this issue, we also employ the quality of the regression and the Gini importance of the traits in each model to define two total importance measures: the total contribution importance ( $IMP_C$ ) and the total Gini importance ( $IMP_G$ ). More specifically,  $IMP_C$  of a trait is defined as the average of  $R_{adj}^2$  values of all models with positive  $R_{adj}^2$  including the trait. This measure captures the contribution of the traits in the models weighted by the performance of the models. The  $IMP_G$  follows the same steps, but the  $R_{adj}^2$  values for each model are also multiplied by the Gini importance of the traits before averaging these values. This total importance measure captures more detail about the impact of the traits on achieving models of good performance while considering the importance of features in the RF model. Having the average values for each trait, we normalize them such that the sum of the importance values of all the traits equals to one. In our analyses, we set the threshold at which a model contributes to the total importance measures as  $R_{adj}^2 = 0$ . This threshold indicates that the model explains the variance of  $g_m$  better than the average of its values (Chicco et al., 2021).

## 493 **6 Data availability**

494 All used data along with the Python functions used in our analyses are available on the following  
495 URL: [github.com/MRahimiMajd/leaf\\_gm\\_architecture](https://github.com/MRahimiMajd/leaf_gm_architecture). The Knauer et al. (2022b) data set is also  
496 available using the link: <https://doi.org/10.6084/m9.figshare.19681410.v1>.

## 497 **7 Funding**

498 All authors acknowledge the funding support by the NovoNordisk Foundation, Data Science Ini-  
499 tiative, project DIRECTION (Grant NNF 21OC0068884, to Z.N. and J.K.).

## 500 **8 Author contributions**

501 M.R.-M. performed analyses, interpreted the results, and wrote the paper. A.L. interpreted results  
502 and commented on drafts of the paper. J.K. interpreted results and commented on the drafts of the  
503 paper. Z.N. conceptualized the study, interpreted results, wrote the paper. All authors contributed  
504 to finalizing the manuscript.

## 505 **9 ORCID**

506 Milad Rahimi-Majd <https://orcid.org/0009-0009-1217-8563>

507 Alistair Leverett <https://orcid.org/0000-0002-7064-1917>

508 Johannes Kromdijk <https://orcid.org/0000-0003-4423-4100>

509 Zoran Nikoloski <https://orcid.org/0000-0003-2671-6763>

## 510 **10 Acknowledgments**

511 The authors would like to thank Dr. Dongliang Xiong for kindly sharing the data on anatomical  
512 and structural leaf architecture traits from  $C_3$  crops.

## 513 **11 Declaration of interest**

514 The authors declare no competing interests.

## 515 **References**

- 516 Carl J Bernacchi, Archie R Portis, Hiromi Nakano, Susanne Von Caemmerer, and Stephen P Long.  
517 Temperature response of mesophyll conductance. implications for the determination of rubisco  
518 enzyme kinetics and for limitations to photosynthesis in vivo. *Plant physiology*, 130(4):1992–  
519 1998, 2002.
- 520 Leo Breiman. Random forests. *Machine learning*, 45:5–32, 2001.
- 521 SV Caemmerer and John R Evans. Determination of the average partial pressure of co2 in chloro-  
522 plasts from leaves of several c3 plants. *Functional Plant Biology*, 18(3):287–305, 1991.
- 523 Marc Carriquí, Miquel Nadal, María J Clemente-Moreno, Jorge Gago, Eva Miedes, and Jaume  
524 Flexas. Cell wall composition strongly influences mesophyll conductance in gymnosperms. *The*  
525 *Plant Journal*, 103(4):1372–1385, 2020.
- 526 Davide Chicco, Matthijs J Warrens, and Giuseppe Jurman. The coefficient of determination r-  
527 squared is more informative than smape, mae, mape, mse and rmse in regression analysis eval-  
528 uation. *PeerJ Computer Science*, 7:e623, 2021.
- 529 Victoria C Clarke, Florence R Danila, and Susanne von Caemmerer. Co2 diffusion in tobacco: a  
530 link between mesophyll conductance and leaf anatomy. *Interface Focus*, 11(2):20200040, 2021.
- 531 María José Clemente-Moreno, Jorge Gago, Pedro Díaz-Vivancos, Agustina Bernal, Eva Miedes,  
532 Panagiota Bresta, Georgios Liakopoulos, Alisdair R Fernie, José Antonio Hernández, and Jaume  
533 Flexas. The apoplastic antioxidant system and altered cell wall dynamics influence mesophyll  
534 conductance and the rate of photosynthesis. *The Plant Journal*, 99(6):1031–1046, 2019.
- 535 E Hance Ellington, Guillaume Bastille-Rousseau, Cayla Austin, Kristen N Landolt, Bruce A Pond,  
536 Erin E Rees, Nicholas Robar, and Dennis L Murray. Using multiple imputation to estimate  
537 missing data in meta-regression. *Methods in Ecology and Evolution*, 6(2):153–163, 2015.
- 538 Patrícia V Ellsworth, Patrick Z Ellsworth, Nuria K Koteyeva, and Asaph B Cousins. Cell wall  
539 properties in oryza sativa influence mesophyll co 2 conductance. *New Phytologist*, 219(1):66–  
540 76, 2018.
- 541 D Epron, D Godard, G Cornic, and B Genty. Limitation of net co2 assimilation rate by internal  
542 resistances to co2 transfer in the leaves of two tree species (fagus sylvatica l. and castanea sativa  
543 mill.). *Plant, Cell & Environment*, 18(1):43–51, 1995.

- 544 GJ Ethier and NJ Livingston. On the need to incorporate sensitivity to co<sub>2</sub> transfer conductance  
545 into the farquhar–von caemmerer–berry leaf photosynthesis model. *Plant, Cell & Environment*,  
546 27(2):137–153, 2004.
- 547 GJ Ethier, NJ Livingston, DL Harrison, TA Black, and JA Moran. Low stomatal and internal  
548 conductance to co<sub>2</sub> versus rubisco deactivation as determinants of the photosynthetic decline of  
549 ageing evergreen leaves. *Plant, Cell & Environment*, 29(12):2168–2184, 2006.
- 550 John R Evans. Mesophyll conductance: walls, membranes and spatial complexity. *New Phytolo-*  
551 *gist*, 229(4):1864–1876, 2021.
- 552 John R Evans and Susanne Von Caemmerer. Temperature response of carbon isotope discrimina-  
553 tion and mesophyll conductance in tobacco. *Plant, Cell & Environment*, 36(4):745–756, 2013.
- 554 JR Evans, TD Sharkey, JA Berry, and GD Farquhar. Carbon isotope discrimination measured con-  
555 currently with gas exchange to investigate co<sub>2</sub> diffusion in leaves of higher plants. *Functional*  
556 *Plant Biology*, 13(2):281–292, 1986.
- 557 Jaume Flexas, María J Clemente-Moreno, Josefina Bota, Tim J Brodribb, Jorge Gago, Yusuke  
558 Mizokami, Miquel Nadal, Alicia V Perera-Castro, Margalida Roig-Oliver, Daisuke Sugiura,  
559 et al. Cell wall thickness and composition are involved in photosynthetic limitation. *Journal of*  
560 *Experimental Botany*, 72(11):3971–3986, 2021.
- 561 Jorge Gago, Marc Carriquí, Miquel Nadal, María José Clemente-Moreno, Rafael Eduardo Coop-  
562 man, Alisdair Robert Fernie, and Jaume Flexas. Photosynthesis optimized across land plant  
563 phylogeny. *Trends in Plant Science*, 24(10):947–958, 2019.
- 564 Lianhong Gu, Stephen G Pallardy, Kevin Tu, Beverly E Law, and Stan D Wullschleger. Reliable  
565 estimation of biochemical parameters from c<sub>3</sub> leaf photosynthesis–intercellular carbon dioxide  
566 response curves. *Plant, Cell & Environment*, 33(11):1852–1874, 2010.
- 567 Peter C Harley, Francesco Loreto, Giorgio Di Marco, and Thomas D Sharkey. Theoretical consid-  
568 erations when estimating the mesophyll conductance to co<sub>2</sub> flux by analysis of the response of  
569 photosynthesis to co<sub>2</sub>. *Plant physiology*, 98(4):1429–1436, 1992.
- 570 Ronald R Hocking. A biometrics invited paper. the analysis and selection of variables in linear  
571 regression. *Biometrics*, pages 1–49, 1976.
- 572 Grace P John, Christine Scoffoni, and Lawren Sack. Allometry of cells and tissues within leaves.  
573 *American Journal of Botany*, 100(10):1936–1948, 2013.

574 Jürgen Knauer, Matthias Cuntz, John R Evans, Ülo Niinemets, Tiina Tosens, Linda-Liisa  
575 Veromann-Jürgenson, Christiane Werner, and Sönke Zaehle. Contrasting anatomical and bio-  
576 chemical controls on mesophyll conductance across plant functional types. *New Phytologist*,  
577 236(2):357–368, 2022a.

578 Jürgen Knauer, Matthias Cuntz, John R. Evans, Ülo Niinemets, Tiina Tosens, Linda-  
579 Liisa Veromann-Jürgenson, Christiane Werner, and Sönke Zaehle. A global dataset of  
580 mesophyll conductance measurements and accompanying leaf traits. 7 2022b. doi:  
581 10.6084/m9.figshare.19681410.v1. URL [https://figshare.com/articles/  
582 dataset/A\\_global\\_dataset\\_of\\_mesophyll\\_conductance\\_measurements\\_  
583 and\\_accompanying\\_leaf\\_traits/19681410](https://figshare.com/articles/dataset/A_global_dataset_of_mesophyll_conductance_measurements_and_accompanying_leaf_traits/19681410).

584 Max Kuhn, Kjell Johnson, et al. *Applied predictive modeling*, volume 26. Springer, 2013.

585 Jihyun Lee and S Natasha Beretvas. Comparing methods for handling missing covariates in meta-  
586 regression. *Research Synthesis Methods*, 14(1):117–136, 2023.

587 J Lloyd, JP Syvertsen, PE Kriedemann, and GD Farquhar. Low conductances for co2 diffusion  
588 from stomata to the sites of carboxylation in leaves of woody species. *Plant, Cell & Environ-*  
589 *ment*, 15(8):873–899, 1992.

590 Francesco Loreto, Peter C Harley, Giorgio Di Marco, and Thomas D Sharkey. Estimation of  
591 mesophyll conductance to co2 flux by three different methods. *Plant physiology*, 98(4):1437–  
592 1443, 1992.

593 Kate Maxwell, Susanne von Caemmerer, and John R Evans. Is a low internal conductance to co2  
594 diffusion a consequence of succulence in plants with crassulacean acid metabolism? *Functional*  
595 *Plant Biology*, 24(6):777–786, 1997.

596 Yusuke Mizokami, KO Noguchi, Mikiko Kojima, Hitoshi Sakakibara, and Ichiro Terashima. Mes-  
597 ophyll conductance decreases in the wild type but not in an aba-deficient mutant (aba1) of n  
598 icotiana plumbaginifolia under drought conditions. *Plant, Cell & Environment*, 38(3):388–398,  
599 2015.

600 F. Pedregosa, G. Varoquaux, A. Gramfort, V. Michel, B. Thirion, O. Grisel, M. Blondel, P. Pretten-  
601 hofer, R. Weiss, V. Dubourg, J. Vanderplas, A. Passos, D. Cournapeau, M. Brucher, M. Perrot,  
602 and E. Duchesnay. Scikit-learn: Machine learning in Python. *Journal of Machine Learning*  
603 *Research*, 12:2825–2830, 2011.

604 José Javier Peguero-Pina, Sergio Sisó, Jaume Flexas, Jeroni Galmés, Ana García-Nogales, Ülo  
605 Niinemets, Domingo Sancho-Knapik, Miguel Ángel Saz, and Eustaquio Gil-Peigrín. Cell-level

606 anatomical characteristics explain high mesophyll conductance and photosynthetic capacity in  
607 sclerophyllous mediterranean oaks. *New Phytologist*, 214(2):585–596, 2017.

608 Soham Raste, Rahul Singh, Joel Vaughan, and Vijayan N Nair. Quantifying inherent randomness  
609 in machine learning algorithms. *arXiv preprint arXiv:2206.12353*, 2022.

610 A Scartazza, M Lauteri, MC Guido, and E Brugnoli. Carbon isotope discrimination in leaf and  
611 stem sugars, water-use efficiency and mesophyll conductance during different developmental  
612 stages in rice subjected to drought. *Functional Plant Biology*, 25(4):489–498, 1998.

613 Ronny Scherer and Valentin Emslander. Quality assessment in meta-analysis (quama). 2023.

614 Thomas D Sharkey. What gas exchange data can tell us about photosynthesis. *Plant, Cell &*  
615 *Environment*, 39(6):1161–1163, 2015.

616 Thomas D Sharkey, Carl J Bernacchi, Graham D Farquhar, and Eric L Singsaas. Fitting pho-  
617 tosynthetic carbon dioxide response curves for c3 leaves. *Plant, cell & environment*, 30(9):  
618 1035–1040, 2007.

619 Padhraic Smyth. Clustering using monte carlo cross-validation. In *Kdd*, volume 1, pages 26–133,  
620 1996.

621 Youshi Tazoe, Susanne Von Caemmerer, Murray R Badger, and John R Evans. Light and co2 do  
622 not affect the mesophyll conductance to co2 diffusion in wheat leaves. *Journal of Experimental*  
623 *Botany*, 60(8):2291–2301, 2009.

624 Youshi Tazoe, Susanne Von Caemmerer, Gonzalo M Estavillo, and John R Evans. Using tunable  
625 diode laser spectroscopy to measure carbon isotope discrimination and mesophyll conductance  
626 to co2 diffusion dynamically at different co2 concentrations. *Plant, Cell & Environment*, 34(4):  
627 580–591, 2011.

628 Magdalena Tomás, Jaume Flexas, Lucian Copolovici, Jeroni Galmés, Lea Hallik, Hipólito  
629 Medrano, Miquel Ribas-Carbó, Tiina Tosens, Vivian Vislap, and Ülo Niinemets. Importance  
630 of leaf anatomy in determining mesophyll diffusion conductance to co2 across species: quanti-  
631 tative limitations and scaling up by models. *Journal of experimental botany*, 64(8):2269–2281,  
632 2013.

633 Tiina Tosens, Keisuke Nishida, Jorge Gago, Rafael Eduardo Coopman, Hernán Marino Cabrera,  
634 Marc Carriquí, Lauri Laanisto, Loreto Morales, Miquel Nadal, Roke Rojas, et al. The pho-  
635 tosynthetic capacity in 35 ferns and fern allies: mesophyll co 2 diffusion as a key trait. *New*  
636 *phytologist*, 209(4):1576–1590, 2016.

- 637 Linda-Liisa Veromann-Jürgenson, Tiina Tosens, Lauri Laanisto, and Ülo Niinemets. Extremely  
638 thick cell walls and low mesophyll conductance: welcome to the world of ancient living! *Jour-*  
639 *nal of Experimental Botany*, 68(7):1639–1653, 2017.
- 640 Linda-Liisa Veromann-Jürgenson, Timothy J Brodribb, Ülo Niinemets, and Tiina Tosens. Vari-  
641 ability in the chloroplast area lining the intercellular airspace and cell walls drives mesophyll  
642 conductance in gymnosperms. *Journal of Experimental Botany*, 71(16):4958–4971, 2020.
- 643 Dongliang Xiong. Leaf anatomy does not explain the large variability of mesophyll conductance  
644 across c3 crop species. *The Plant Journal*, 113(5):1035–1048, 2023.
- 645 Xinyou Yin and Paul C Struik. Theoretical reconsiderations when estimating the mesophyll con-  
646 ductance to co2 diffusion in leaves of c3 plants by analysis of combined gas exchange and  
647 chlorophyll fluorescence measurements. *Plant, Cell & Environment*, 32(11):1513–1524, 2009.
- 648 Xinyou Yin, Paul C Struik, Pascual Romero, Jeremy Harbinson, Jochem B Evers, Peter EL Van  
649 Der Putten, and JAN Vos. Using combined measurements of gas exchange and chlorophyll flu-  
650 orescence to estimate parameters of a biochemical c3 photosynthesis model: a critical appraisal  
651 and a new integrated approach applied to leaves in a wheat (*triticum aestivum*) canopy. *Plant,*  
652 *cell & environment*, 32(5):448–464, 2009.
- 653 Xin-Guang Zhu, Stephen P Long, and Donald R Ort. Improving photosynthetic efficiency for  
654 greater yield. *Annual review of plant biology*, 61:235–261, 2010.

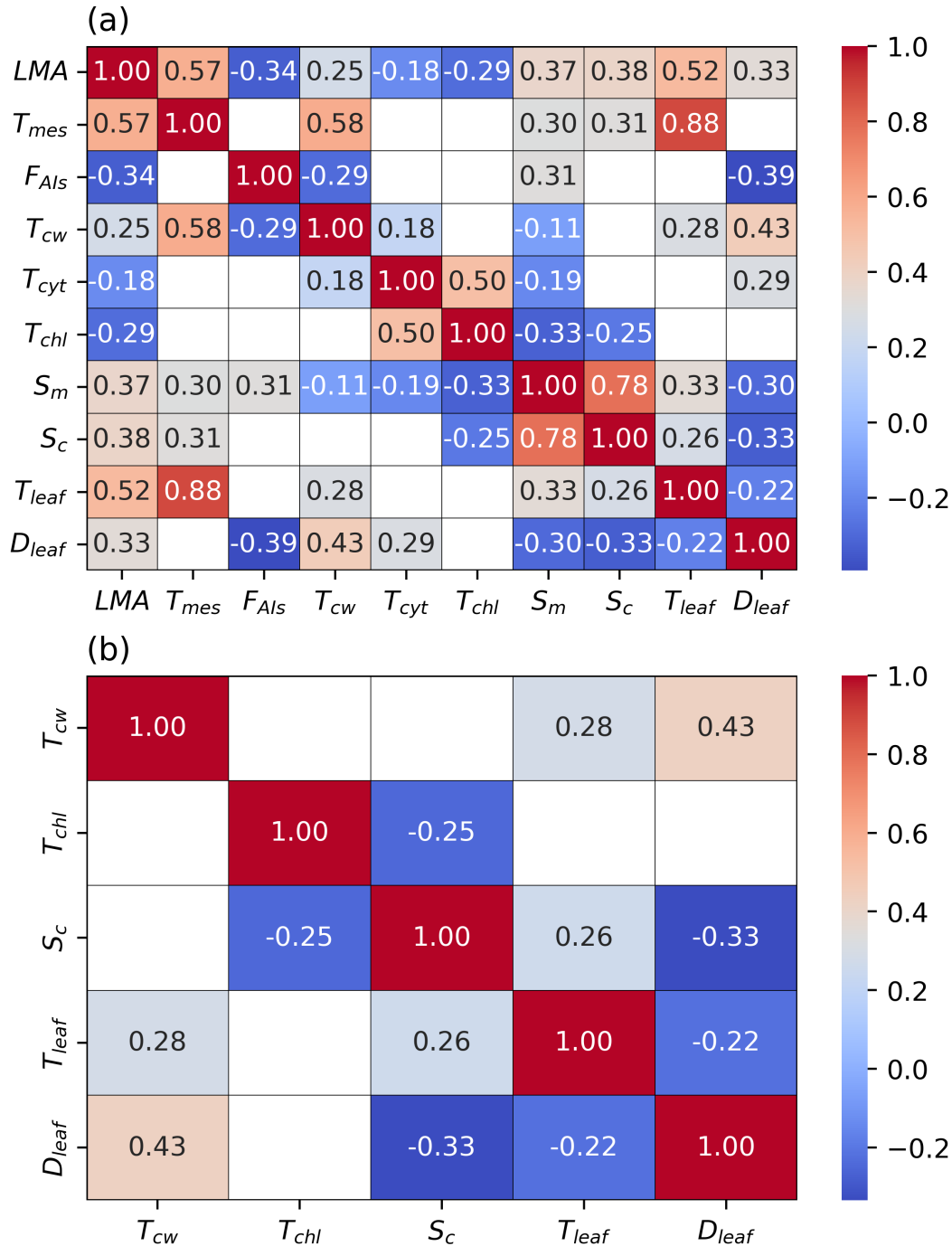


**Figure 2: Correlation structure of anatomical traits.** Pearson correlation between a) all anatomical traits and b) the anatomical traits of the best-performing model for cross-validation on the global data set. The correlation was calculated on the available data for each trait pair, regardless of other traits. Missing entries in matrices indicate that the p-value of the correlation was larger than our considered significance level 0.05.

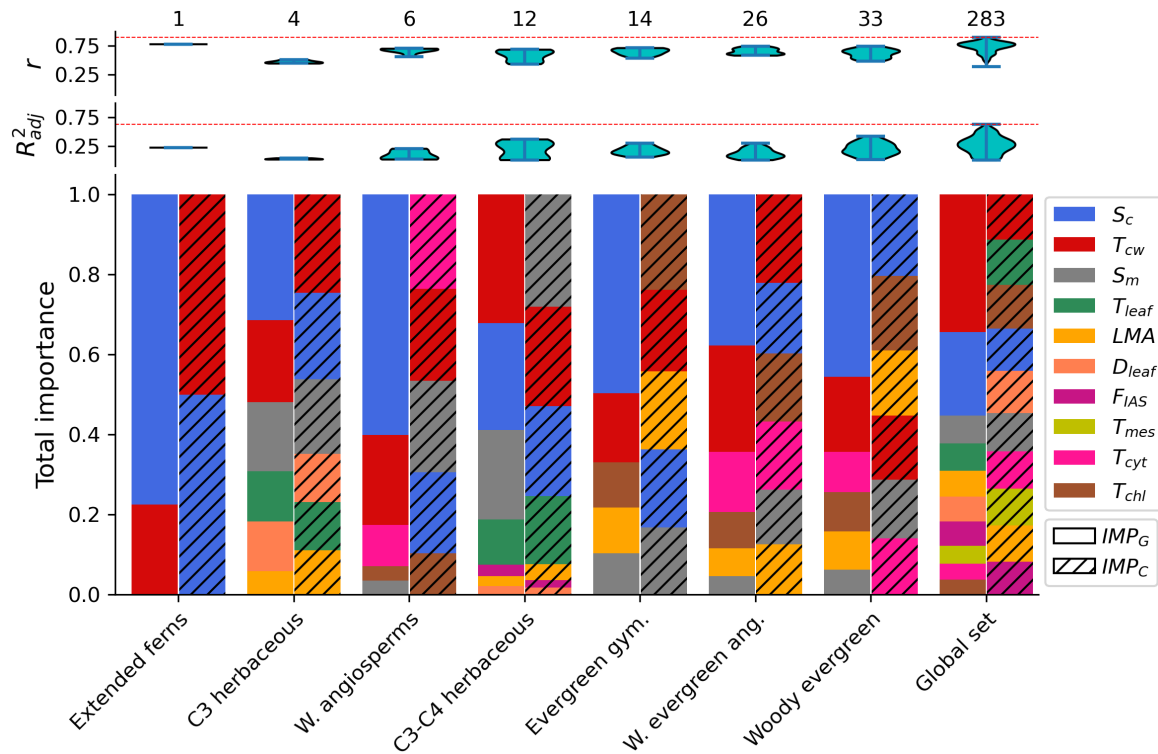


**Figure 3: The predictive performance and total feature importance ratios of the trained models within PFTs.** Evaluation of the performance of models in different prediction scenarios based on cross-validation within different PFTs. The upper panels show the violin plots of the average predictability scores ( $r$  and  $R_{adj}^2$ ) of the models for the global data set and each PFT. The number of models with positive  $R_{adj}^2$  in each scenario is given above the violin plots. The dashed red lines indicate the maximum predictability scores across all models. The bar charts in the lower panel show the total importance measures,  $IMP_C$  and  $IMP_G$ , of the contributing traits in the models of the global data set and individual PFTs. The position of traits in the bar charts has been sorted from top to bottom based on their total importance. For all the cases, the average predictability scores were achieved by RF model in 150 executions, with 70% randomly chosen data elements used for the training set and the remaining 30% used for the test set.

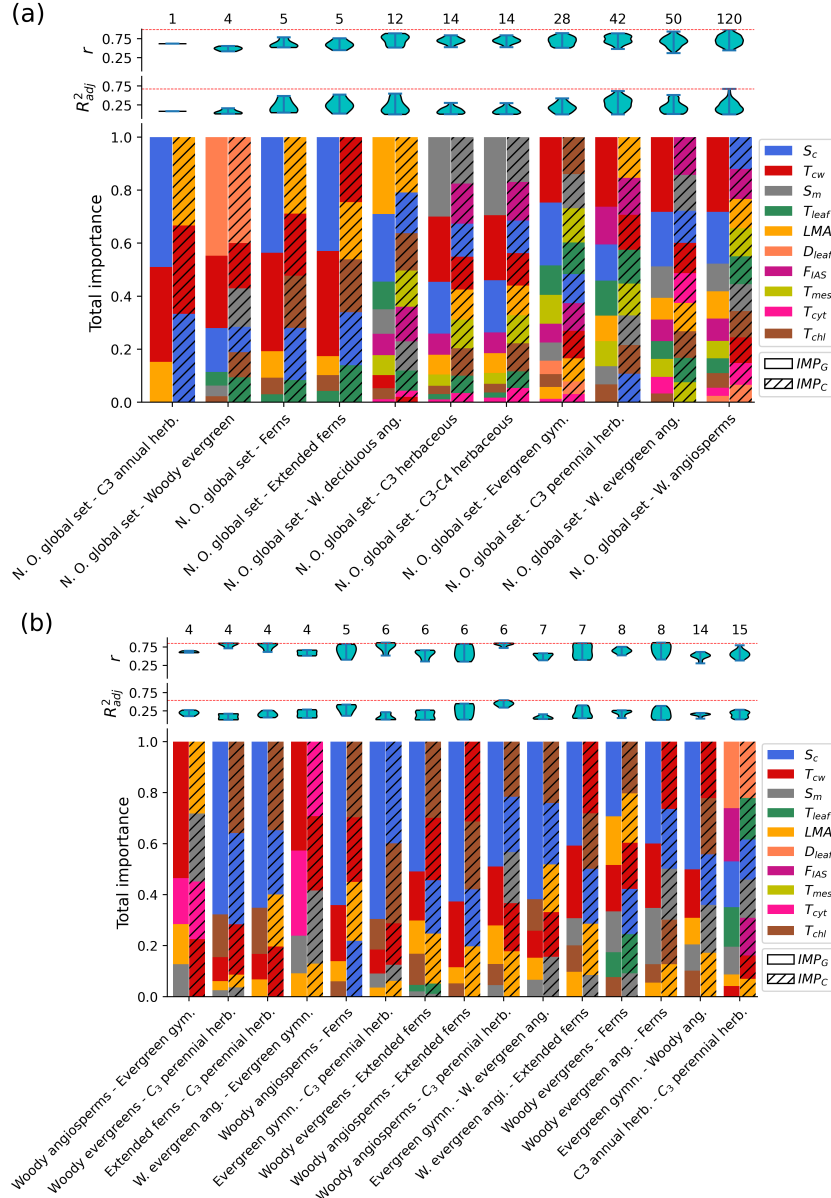


**Figure 4: The predictive performance and total feature importance ratios of the trained models between PFTs.** The evaluation of the performance of the models in different prediction scenarios with the test sets of individual PFTs and the training sets of: a) non-overlapping global data set with corresponding test sets and b) other individual PFTs. Figure b) contains the 15 of the 31 scenarios with at least one model with a positive  $R^2_{adj}$ . The rest of the scenarios are illustrated in Fig. S4. The upper panels show the violin plots of the average predictability scores ( $r$  and  $R^2_{adj}$ ) of the models for each prediction scenario. The number of models with positive  $R^2_{adj}$  in each scenario is given above the violin plots. The dashed red lines indicate the maximum of predictability scores across all the models. The bar charts in the lower panels show the total importance measures,  $IMP_C$  and  $IMP_G$ , of the contributing traits in the models of each scenario. The position of traits in the bar charts has been sorted from top to bottom based on their total importance. For all models, the average predictability scores and importance ratios were achieved by RF model in 50 executions, with the fixed training and test sets.

**Table 2: Best-performing models for  $g_m$  between PFTs.**

Prediction scenario	$R_{adj}^2$	$r$	$n$
Non-overlapping global set - Woody angiosperms	0.67	0.84	371
Non-overlapping global set - $C_3$ perennial herbaceous	0.62	0.85	83
Non-overlapping global set - Woody deciduous ang.	0.55	0.89	210
Non-overlapping global set - Extended ferns	0.52	0.76	57
Non-overlapping global set - Woody evergreen ang.	0.51	0.94	387
Non-overlapping global set - Ferns	0.49	0.79	55
Non-overlapping global set - Evergreen gym.	0.42	0.84	442
Non-overlapping global set - $C_3$ herbaceous	0.30	0.81	441
Non-overlapping global set - $C_3 - C_4$ herbaceous	0.30	0.81	436
Non-overlapping global set - Woody evergreens	0.16	0.56	171
Non-overlapping global set - $C_3$ annual herbaceous	0.09	0.62	347
Woody angiosperms - $C_3$ perennial herbaceous	0.54	0.86	40
Woody angiosperms - Extended ferns	0.45	0.79	30
Woody angiosperms - Ferns	0.42	0.83	30
Woody evergreen angiosperms - Extended ferns	0.40	0.85	23
Woody evergreen angiosperms - Ferns	0.38	0.86	23
$C_3$ annual herbaceous - $C_3$ perennial herbaceous	0.28	0.63	37
Woody evergreen angiosperms - Evergreen gymnosperms	0.28	0.67	35
Woody evergreens - Ferns	0.26	0.66	47
Woody evergreens - Extended ferns	0.27	0.66	43
Woody angiosperms - evergreen gymnosperms	0.27	0.65	55
Extended ferns - $C_3$ perennial herbaceous	0.26	0.84	16
Evergreen gymnosperms - $C_3$ perennial herbaceous	0.21	0.87	23
Evergreen gymnosperms - Woody angiosperms	0.19	0.52	29
Woody evergreens - $C_3$ perennial herbaceous	0.17	0.85	65
Evergreen gymnosperms - Woody evergreen angiosperms	0.16	0.48	30

Predictability scores of the models with the highest  $R_{adj}^2$  for 9 prediction scenarios between the non-overlapping global data set and different PFTs (upper side) and 15 prediction scenarios between different PFTs (lower side), with at least one model with a positive  $R_{adj}^2$ . The number of trained models for each scenario is also given in the table by  $n$ .

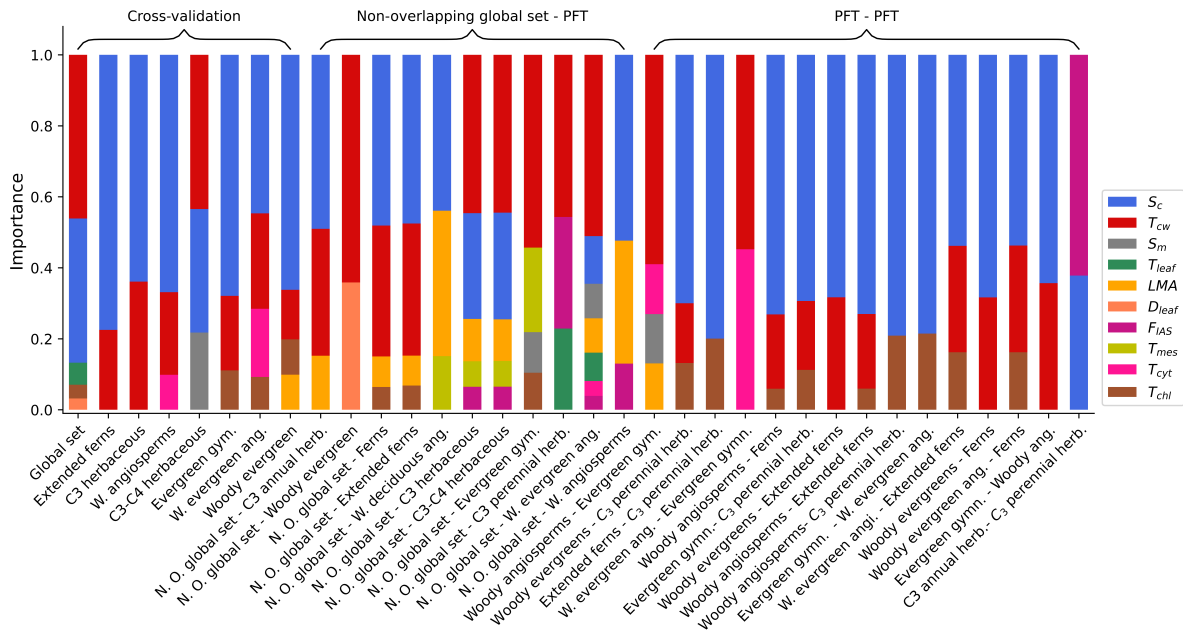


**Figure 5: The importance of the traits in the best models of different prediction scenarios.** The average Gini importance of the contributing traits on the optimal models of different prediction scenarios, based on  $R_{adj}^2$ . The position of traits in the bar charts has been sorted from top to bottom based on their relative importance. The prediction scenarios were classified into three groups based on the data splitting methods: *i*) cross-validation scenarios, *ii*) scenarios with the individual PFTs as the test sets and the non-overlapping part of the global data set with them as the training set, and *iii*) scenarios in which the training and test sets are non-overlapping individual PFTs.

# Supplemental information

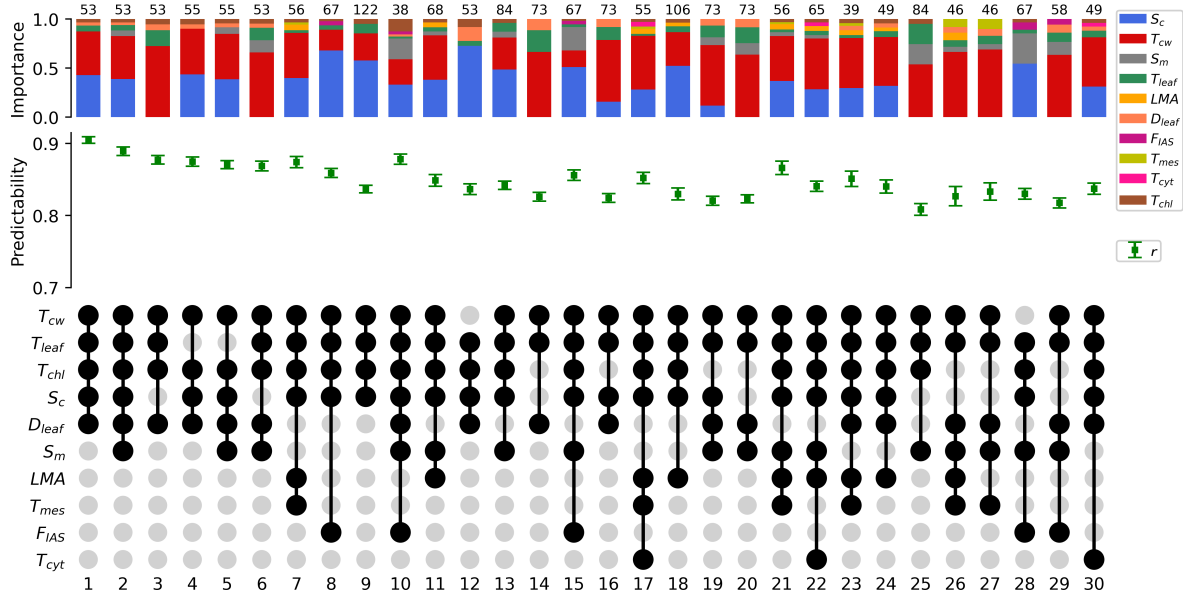


**Figure S1: Predictive performance of random forest models, with at least 25 data points, using different combinations of leaf anatomical traits.** The UpSet plot shows the predictability evaluation of top 30 models, with 25 data points or more, for  $g_m$ , based on average  $r$ , consisting of ten anatomical traits  $LMA$ ,  $T_{mes}$ ,  $F_{IAS}$ ,  $T_{cw}$ ,  $T_{cyt}$ ,  $T_{chl}$ ,  $S_m$ ,  $S_c$ ,  $T_{leaf}$ , and  $D_{leaf}$  over all available species and PFTs of Knauer et al. (2022b) data set. The lower panel shows the intersection of traits contributing to the training model. The middle panel indicates the average  $r$  between the measured and predicted values of  $g_m$  in the test set. The error bars show the standard errors of the predictability measures. The upper panel shows the average Gini importance of the corresponding traits at each combination of the traits. The number of data points in each model is provided above the importance bars. For all models, the average predictability scores were achieved by the RF model in 150 executions, with 70% randomly chosen data elements used for the training set and the remaining 30% used for the test set.

**Table S1: Available data for anatomical traits.**

	Trait	No. of data points
1	Leaf dry mass per area ( $gm^{-2}$ )	712
2	Surface area of chloroplasts exposed to the intercellular airspaces per unit leaf area ( $m^2m^{-2}$ )	408
3	Surface area of mesophyll cells exposed to the intercellular airspaces per unit leaf area ( $m^2m^{-2}$ )	377
4	Cell wall thickness ( $\mu m$ )	362
5	Leaf thickness ( $\mu m$ )	346
6	Chloroplast thickness ( $\mu m$ )	237
7	Fraction of intercellular airspaces in leaf mesophyll	225
8	Mesophyll thickness ( $\mu m$ )	191
9	Leaf density ( $g\ cm^{-3}$ )	170
10	Cytosol thickness ( $\mu m$ )	131
11	Stomatal density abaxial ( $mm^{-2}$ )	111
12	Stomatal density adaxial ( $mm^{-2}$ )	84
13	Chloroplast length ( $\mu m$ )	79
14	Palisade mesophyll thickness ( $\mu m$ )	71
15	Spongy mesophyll thickness ( $\mu m$ )	71
16	Stomatal density ( $mm^{-2}$ )	52
17	Single stomatal area on abaxial leaf side ( $\mu m^2$ )	39
18	Single stomatal area ( $\mu m^2$ )	33
19	Leaf width ( $mm$ )	33
20	Epidermis thickness on adaxial leaf side ( $\mu m$ )	31
21	Single stomatal area on adaxial leaf side ( $\mu m^2$ )	31
22	Stomatal length on abaxial leaf side ( $\mu m$ )	31
23	Stomatal length on adaxial leaf side ( $\mu m$ )	30
24	Epidermis thickness on abaxial leaf side ( $\mu m$ )	30
25	Interveinal distance ( $\mu m$ )	26
26	Stomatal length ( $\mu m$ )	24
27	Stomatal width ( $\mu m$ )	22
28	Stomatal index (%)	21
29	Chloroplast surface area ( $\mu m^2$ )	16
30	Chloroplast width ( $\mu m$ )	14
31	Surface area of bundle sheath cells per unit leaf area ( $m^2m^{-2}$ )	7

The number of data points in the data set of Knauer et al. (2022a) for all measured anatomical traits. Due to the size of the available data points, we used the first ten traits in our analyses.

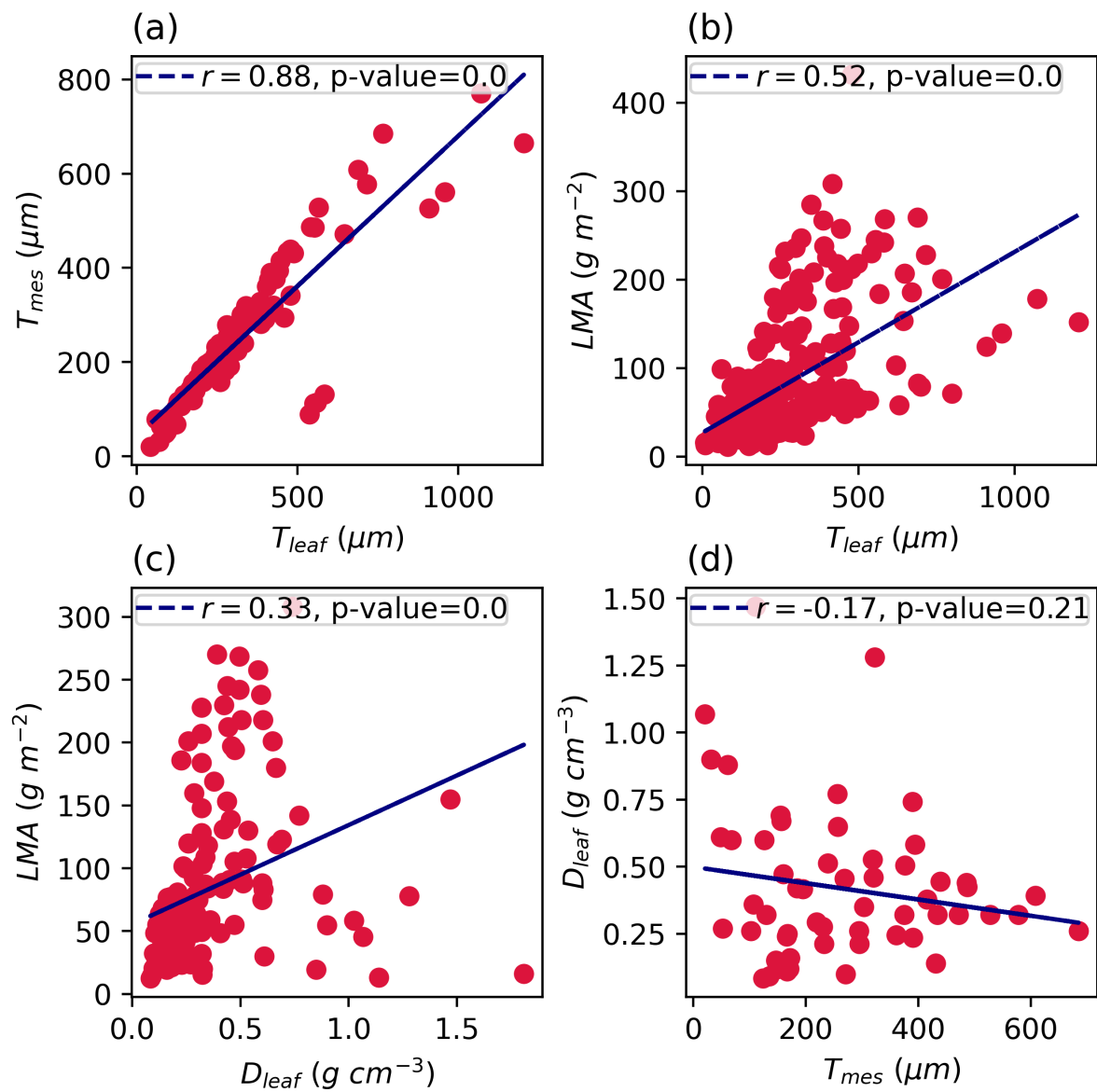


**Figure S2: Linear regression between different anatomical traits.** Linear regression between the pairs of anatomical traits: a)  $T_{leaf}$  and  $T_{mes}$ , b)  $T_{leaf}$  and  $LMA$ , c)  $D_{leaf}$  and  $LMA$ , and d)  $T_{mes}$  and  $LMA$ .

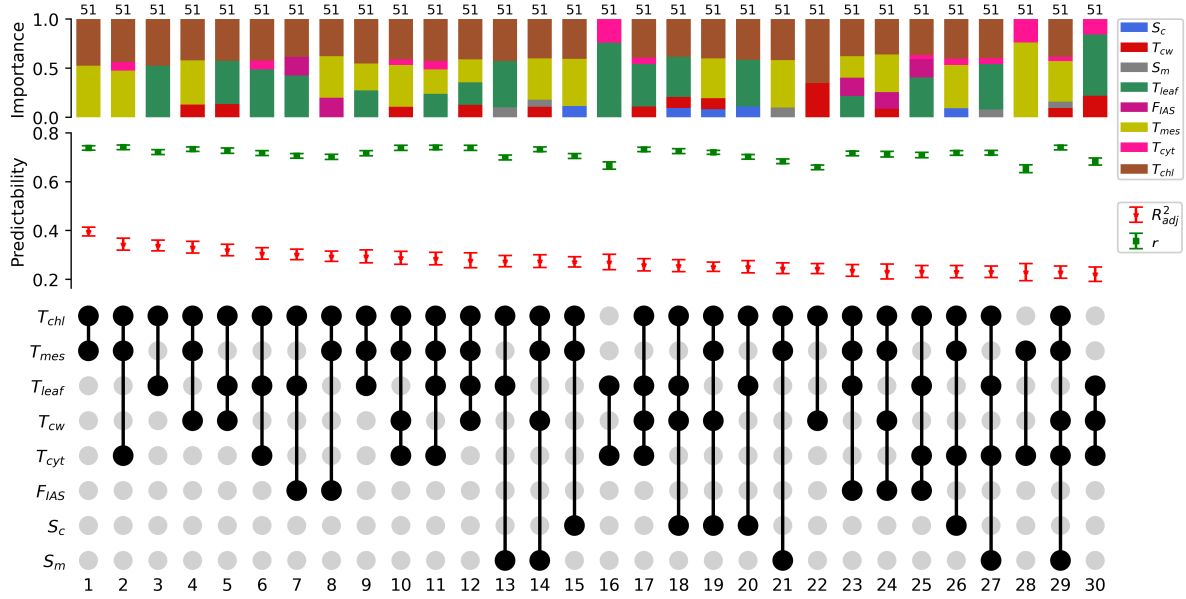


**Figure S3: Predictive performance of random forest models using different combinations of leaf anatomical traits.** The UpSet plot shows the predictability evaluation of top 30 models for  $g_m$ , based on average  $R^2_{adj}$ , consisting of eight anatomical and structural traits  $T_{mes}$ ,  $F_{IAS}$ ,  $T_{cw}$ ,  $T_{cyt}$ ,  $T_{chl}$ ,  $S_m$ ,  $S_c$ , and  $T_{leaf}$  over all available species of Xiong (2023) data set. The lower panel shows the intersection of traits contributing to the training model. The middle panel indicates the average  $R^2_{adj}$  and  $r$  between the measured and predicted values of  $g_m$  in the test set. The error bars show the standard errors of the predictability measures. The upper panel shows the average Gini importance of the corresponding traits at each combination of the traits. The number of data points in each model is provided above the importance bars. For all models, the average predictability scores were achieved by the RF model in 150 executions, with 70% randomly chosen data elements used for the training set and the remaining 30% used for the test set. The data set consists of ten  $C_3$  crops, glycine max, oryza sativa, arundo donax, helianthus annuus, triticum aestivum, gossypium hirsutum, beta vulgaris, astragalus sinicus, lycopersicon esculentum, and solanum tuberosum, where our  $C_3$  data set contain the first 6 species.

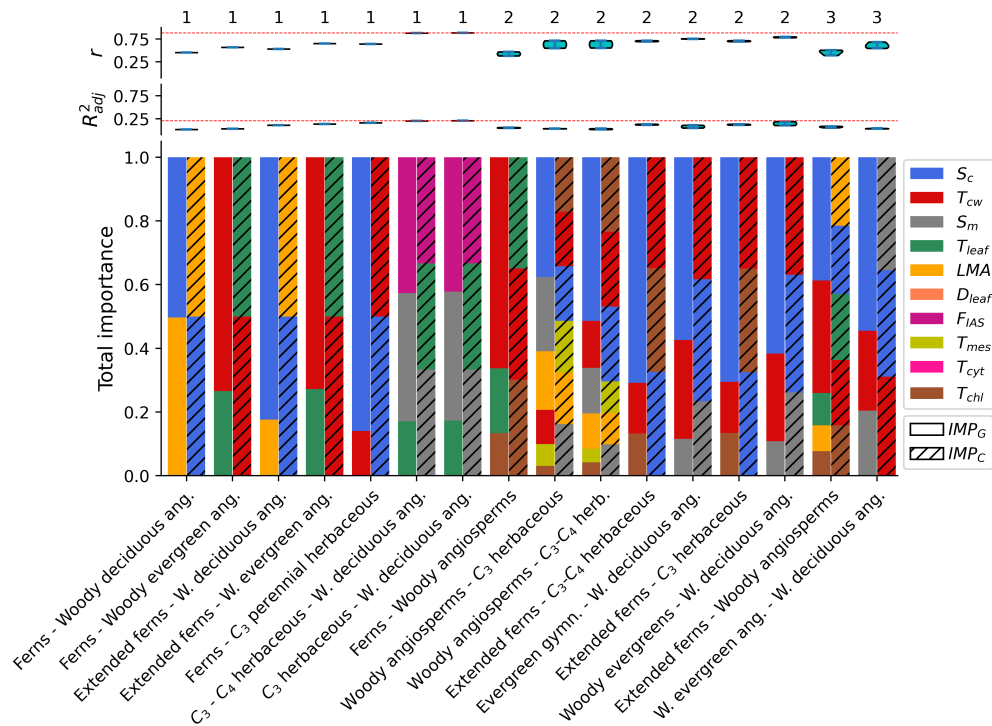


**Figure S4: The predictive performance and total feature importance ratios of the trained models between PFTs.** The evaluation of the performance of the models in 16 prediction scenarios with the test sets of individual PFTs and the training sets of other individual PFTs. The figure shows the results for the rest of the scenarios shown in Fig. 4b. The upper panels show the violin plots of the average predictability scores ( $r$  and  $R_{adj}^2$ ) of the models for each prediction scenario. The number of models with positive  $R_{adj}^2$  in each scenario is given above the violin plots. The dashed red lines indicate the maximum of predictability scores across all the models. The bar charts in the lower panel show the total importance measures,  $IMP_C$  and  $IMP_G$ , of the contributing traits in the models of each scenario. The position of traits in the bar charts has been sorted from top to bottom based on their total importance. For all models, the average predictability scores and importance ratios were achieved by RF model in 50 executions, with the fixed training and test sets.

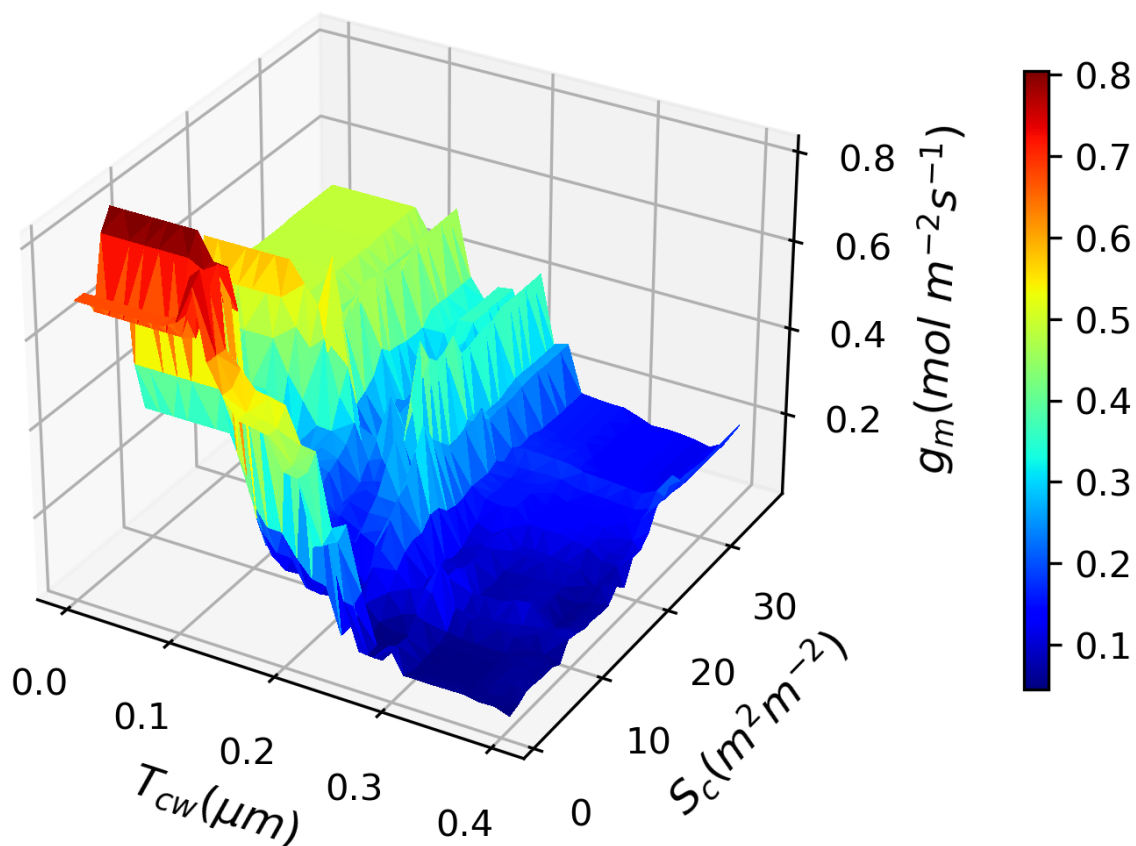


**Figure S5: Variation of  $g_m$  based on  $T_{cw}$  and  $S_c$**  The surface plot of  $g_m$  based on a trained model on  $T_{cw}$  and  $S_c$ . The model was built by cross-validation on the global data set with 70% randomly chosen data elements used for the training set and the remaining 30% used for the test set. After training the model, 30 equally spaced data points were determined for each of the predictors, and then  $g_m$  values were predicted for all 900 pairs of  $T_{cw}$  and  $S_c$  data points. The ranges of both predictors were based on their minimum and maximum in the test set, except for the maximum of  $T_{cw}$  where we reduced it to 0.4 to indicate the fluctuations of  $g_m$ .

**Table S2: The statistics of the data for global data set and individual PFTs.**

Plant functional type	No. of data samples	No. of species	No. of $n \geq 50$
global data set	882	453	599
$C_3 - C_4$ herbaceous	382	116	49
$C_3$ herbaceous	354	93	49
Woody evergreens	302	214	72
Woody angiosperms	287	185	72
$C_3$ annual herbaceous	255	35	22
Woody evergreen angiosperms	176	122	63
Evergreen gymnosperms	126	92	31
Woody deciduous angiosperms	108	60	1
$C_3$ perennial herbaceous	99	58	2
Extended ferns	64	44	7
Ferns	58	39	1
$C_4$ annual herbaceous	17	12	0
$C_4$ perennial herbaceous	11	11	0
Deciduous gymnosperms	10	4	0
Mosses	10	10	0
Fern allies	6	5	0
Semi-deciduous angiosperms	3	3	0
CAM plants	3	2	0

The number of data samples with a value for  $g_m$  and at least one of the anatomical traits for the global data set and different PFTs are provided in the first column. The second column shows the number of species contributing to each set. The number of combinations with at least 50 data points in each set is given in the following column.